Cosmic evolution through UV surveys (CETUS): point spread function analysis of three mirror anastigmat telescope

Ashcraft, Jaren, Choi, Heejoo, Heap, Sara, Woodruff, Robert, Kim, Dae Wook

Jaren N. Ashcraft, Heejoo Choi, Sara R. Heap, Robert A. Woodruff, Dae Wook Kim, "Cosmic evolution through UV surveys (CETUS): point spread function analysis of three mirror anastigmat telescope," Proc. SPIE 11820, Astronomical Optics: Design, Manufacture, and Test of Space and Ground Systems III, 118200H (24 August 2021); doi: 10.1117/12.2598879

SPIE.

Event: SPIE Optical Engineering + Applications, 2021, San Diego, California, United States

Cosmic Evolution through UV Surveys (CETUS): Point Spread Function Analysis of Three Mirror Anastigmat Telescope

Jaren N. Ashcraft[a], Heejoo Choi[a,c], Sara R. Heap[d], Robert A. Woodruff[e], and Daewook Kim[a,b,c]

[a]Wyant College of Optical Sciences, 1630 E University Blvd, Tucson, AZ 85721
[b]Steward Observatory, 933 N Cherry Ave, Tucson, AZ 85719
[c]Large Binocular Telescope Observatory, University Of Arizona, 933 N. Cherry Ave. Tucson, AZ 85721
[d]Department of Astronomy, University of Maryland, College Park, MD
[e]Woodruff Consulting, 2081 Evergreen Ave., Boulder, CO

ABSTRACT

Cosmic Evolution through UV Surveys (CETUS) is a concept for a UV space telescope that was studied with funding from NASA. The CETUS Final Report is posted at arXiv: 1909.10437, but post-report studies are continuing. Here, we describe telescope design options for CETUS including a trade study between a traditional on-axis three-mirror anastigmat (TMA) and freeform off-axis TMA solution considering their alignment sensitivity and tolerances. Different secondary support structures are explored for the on-axis design to analyze the irradiance distribution of the point-spread function (PSF) due to the pupil obscuration and how it influences the simulated starfield at the telescope focal planes. With rigorous and judicious analysis in geometrical optical design and physical wave propagation modeling, we aim to enable the next generation of spaceborne optical observatory for UV astronomy.

Keywords: space telescope, ultraviolet, freeform, diffraction, linear astigmatism

1. INTRODUCTION

Throughout its 31-year lifetime the Hubble Space Telescope (HST) has enabled astronomers to observe the universe in the UV. HST's orbit is well above the earth's atmosphere, making it an integral tool for UV astronomy. Given HST's age, there is a clear need for the advancement of UV-sensitive technology to provide astronomers with the tools they need in the post-Hubble era.[1] CETUS is a probe-class mission concept tailored to high-sensitivity observations in the UV. This observatory is principally concerned with the imaging and characterization of faint diffuse, extended sources like the circumgalactic medium (CGM) that inform the processes of galactic evolution. CETUS is also well-equipped to provide support for transient phenomena observed by other observatories (e.g. the Vera Rubin telescope) and follow-up observations to be made in other wavebands (e.g. Roman, Subaru, Euclid, ALMA). To satisfy these goals, a three-mirror anastigmat was designed to deliver a wide field of view (17.4'x17.4') at a fast focal ratio (F/5) to a suite of spectroscopic and imaging instruments capable of resolving and characterizing diffuse sources like the CGM. CETUS should be 22 times more sensitive than the slower focusing HST ($F/24$) to extended sources.[2] However, this comparison assumes that the ability of HST and CETUS to resolve the sources is otherwise equal. Diffraction from structure in the pupil (secondary supports, surface errors) must be considered to properly evaluate the optical performance of the CETUS telescope (shown in figure 1).

Further author information: (Send correspondence to J.N.A.)
J.N.A.: E-mail: jashcraft@email.arizona.edu
D.W.K.: E-mail: dkim@optics.arizona.edu

Astronomical Optics: Design, Manufacture, and Test of Space and Ground Systems III, edited by Tony B. Hull, Daewook Kim, Pascal Hallibert, Fanny Keller, Proc. of SPIE Vol. 11820, 118200H · © 2021 SPIE
CCC code: 0277-786X/21/$21 · doi: 10.1117/12.2598879

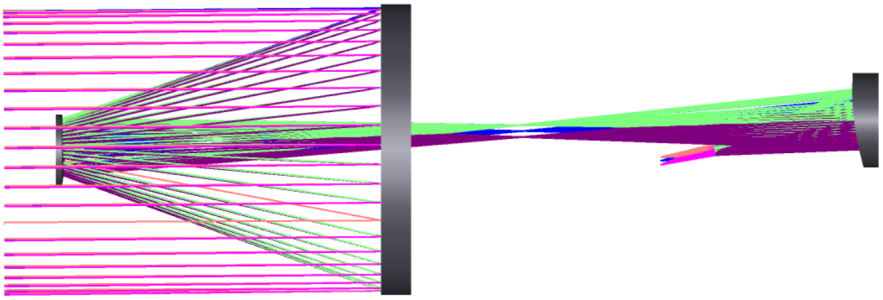

Figure 1. The original design of CETUS's fore-optics, a three-mirror anastigmat with an elliptical primary, hyperbolic secondary, and elliptical tertiary. CETUS biases the field of view so that an on-axis detector doesn't vignette the incoming light.

Such an investigation into diffraction-limited resolution is easily done numerically, and has been conducted previously by software packages such as Tiny TIM[3] and WebbPSF[4] to simulate the point-spread functions of the HST and JWST respectively. The diffraction performance of CETUS will be analyzed using the physical optics engine of WebbPSF: Physical Optics Propagation in Python (POPPY). POPPY is an object-oriented open source physical optics engine developed by the Space Telescope Science Institute that supports Fraunhofer and Fresnel diffraction modeling with a wide library of optical element models. Feng et al[5] recently used POPPY to investigate the effects of pupil segmentation on the fractional encircled energy radius for an on-axis image point. The same analysis can be applied to a circular pupil obscured by a secondary mirror with structural supports. This will reveal how structure in the pupil can influence the sensitivity of CETUS to faint sources by demonstrating how the energy from a point on the object is distributed in the image plane. A rough optical surface phase can also be applied to the primary to bring the physical optics model closer to the as-built performance using a real mirror surface. Four aperture geometries were considered for the CETUS diffraction simulation: The original on-axis CETUS spider, two Hubble-like spiders, and an unobscured pupil. These aperture geometries are shown in figure 2

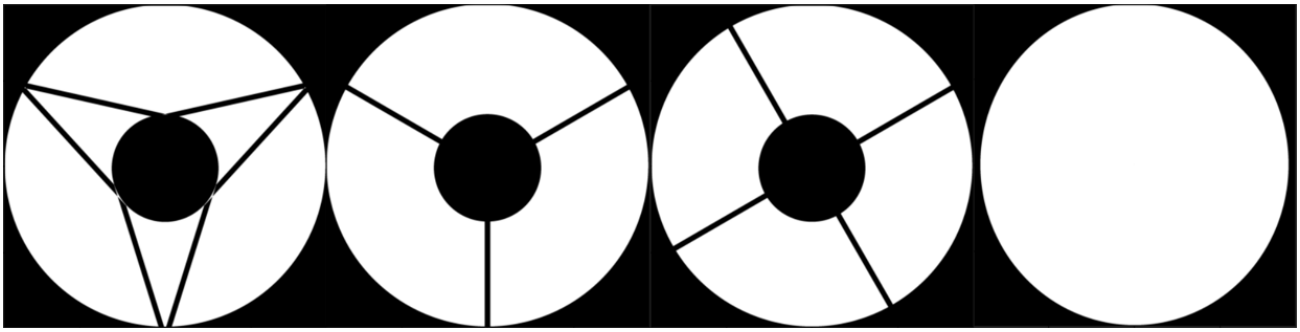

Figure 2. Aperture geometries investigated from left to right: The original on-axis CETUS spider, a Hubble-like spider with 3 spokes, a Hubble-like spider with 4 spokes, an Unobscured pupil.

The goal of using these pupils is to compare the current spider design (Original), alternative spider geometries (Hubble 3x/4x), and an unobscured primary mirror. However, there is no way to make the the original optical system shown in figure 1 unobscured without fundamentally changing the optical design. A new unobscured design was conceived leveraging insights from freeform optical design as a candidate set of CETUS fore-optics that could operate without diffraction from pupil structure, should these features be the factor limiting resolution.

2. AN UNOBSCURED SOLUTION FREE OF LINEAR ASTIGMATISM

An unobscured geometry for the CETUS fore-optics was proposed as a method to eliminate all diffraction flares from the secondary support structure obscuring the pupil. To remove all obscurations by the secondary mirror, the primary was turned into an off-axis parabola. Following Sasian's method of confocal mirror design[6] an unobscured three-mirror anastigmat was designed that met the packaging requirements of the CETUS fore-optics. The resultant system has plane-symmetry about the $\hat{x}-\hat{z}$ plane, which grants the anastigmat simmilarly symmetric performance across the field of view. However, to achieve comparable performance to the original design freeform coefficients are necessary. To optimize the freeform coefficients effectively the linear astigmatism of the design must be controlled.

$$\frac{l_2'}{l_2}\frac{l_3'}{l_3}tani_1 + \left(1+\frac{l_2'}{l_2}\right)\frac{l_3'}{l_3}tani_2 + \left(1+\frac{l_3'}{l_3}\right)tani_3 = 0 \tag{1}$$

Equation 1 is a constraint on the front ($l_{2,3}$) and rear ($l'_{2,3}$) focal distances of the conic mirrors, as well as the angles of incidence of the optical axis ray ($i_{1,2,3}$) on each surface in the $\hat{x}-\hat{z}$ plane. When this condition is zero-valued linear astigmatism is not present in the optical system. This is suitable for freeform design starting solutions because linear astigmatism is a very strong aberration present when the rotational symmetry of the optical system is broken. Eliminating it with the system geometry allows for more convergent optimization of freeform coefficients on each surface in the system. To maintain the field-symmetric performance the surfaces were optimized with XY-Polynomials with an aspheric departure described by equation 2

$$Sag = \frac{cr^2}{1+\sqrt{1-(1+k)c^2r^2}} + \sum_{i=1}^{N} A_i E_{x,y}^i \tag{2}$$

Where the sum represents a power series in $\hat{x}$ and $\hat{y}$. Selectively optimizing the coefficients (A_i) of this power series enables control on the symmetry of the aberrated field in the $\hat{x}$ and $\hat{y}$ directions. Optimizing only coefficients of even order in $\hat{x}$ maintains the plane-symmetric performance of the system, while allowing the coefficients of any order in $\hat{y}$ to correct for the aberrations induced by breaking the rotational symmetry in that direction. The resultant anastigmat is shown in figure 3

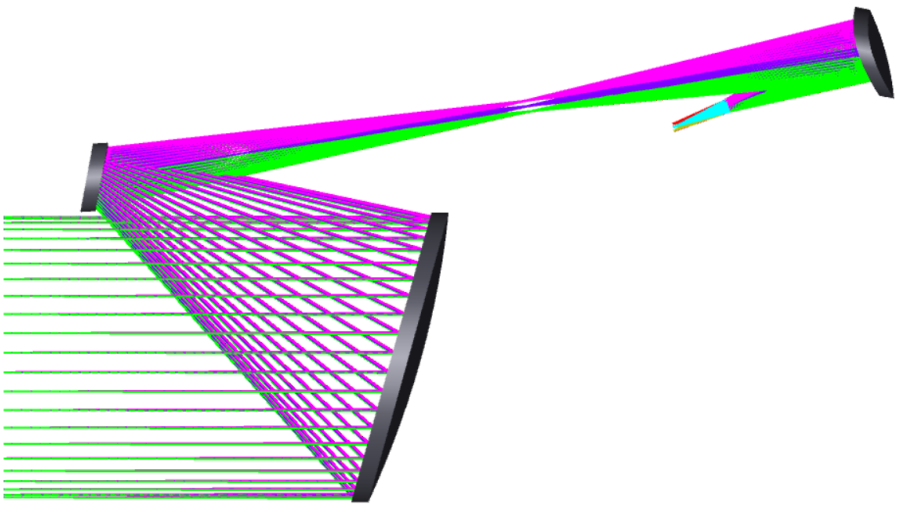

Figure 3. The unobscured realization of the CETUS fore-optics. All mirrors in this system are XY-Polynomial surfaces. The primary mirror is slightly undersized to be equivalent in collecting area to the original on-axis design.

The CETUS focal plane is partitioned into two $17.4'x17.4'$ focal planes symmetric about the $\hat{x}-\hat{z}$ plane separated by $48.6'$ (Figure 4). The additional degrees of freedom granted by freeform optical surfaces grant considerable aberration correction in the focal plane region by taking advantage of the plane-symmetric image.

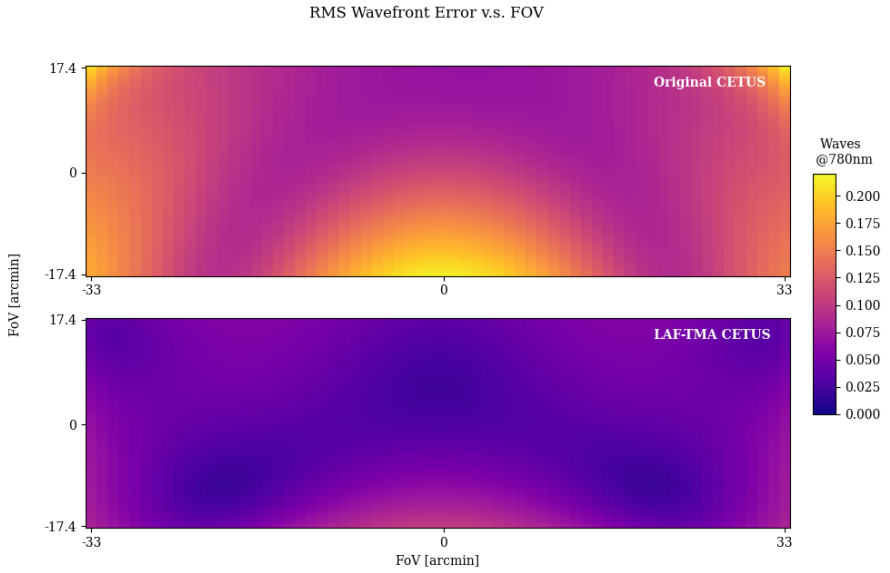

Figure 4. RMS WFE v.s. field of view plots with the same scale comparing the on-axis (Top) and off-axis (Bottom) designs. The RMS WFE in the detector region is 0.124 waves for the on-axis and 0.048 waves for the off-axis.

The performance shown in figure 4 mirrors the geometry of each system. The original CETUS design utilizes rotationally-symmetric optics with a biased field of view, resulting in a shifted rotationally-symmetric performance. The off-axis design's bilaterally symmetric surfaces generate similarly bilaterally symmetric performance as a function of field-of-view. The wavefront error fields are plotted on the same scale for comparison, showing that the off-axis design nominally performs better across the field of view. The freeform departure is shown in figure 5.

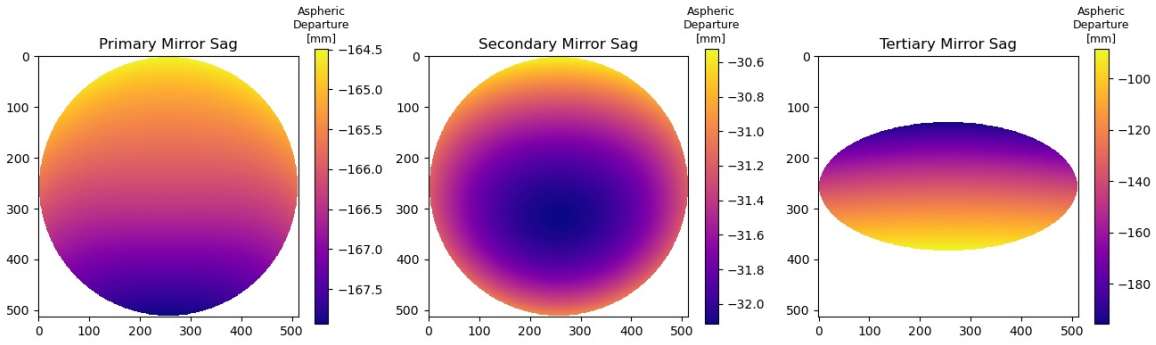

Figure 5. Aspheric departure of the Primary (Left), Secondary (Center), and Tertiary (Right) mirrors. The base radius and tilt are removed from these mirrors.

The performance may be great, but this comes at the cost of more complex surfaces and consequently, more complex alignment. To quantify how significant the alignment burden would be for the off-axis design a sensitivity analysis is performed for each element in each system. An optic in the system is perturbed in six degrees of freedom individually. The RMS Spot Radius in arcseconds was recorded at each step and plotted against a conservative figure of merit at 0.225 arcseconds (The performance criterion is 0.25 arcsecond spot radius). The sensitivity is reported as the perturbation in one degree of freedom required to achieve an RMS spot radius equal to the figure of merit, and are reported in figure 6.

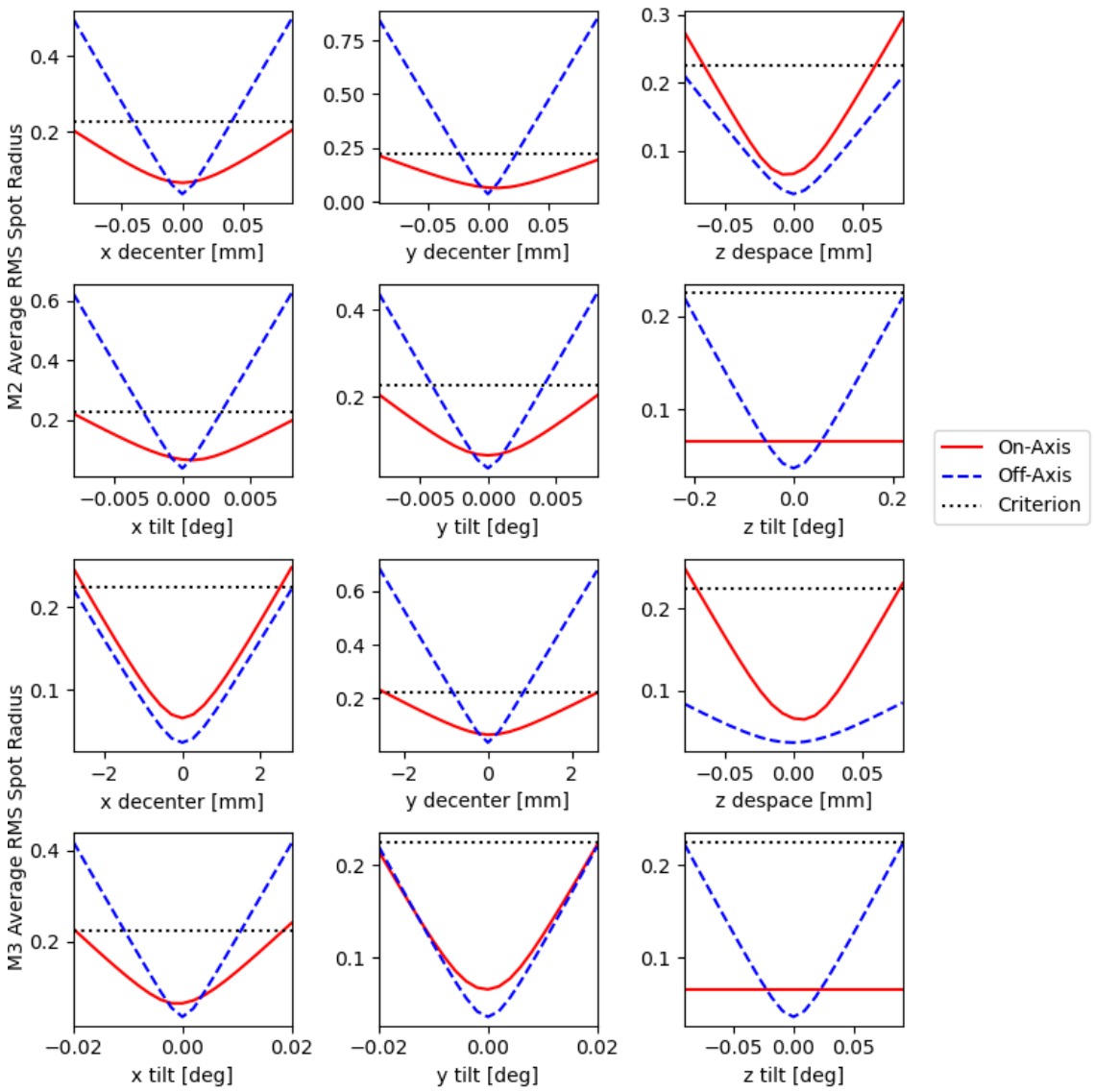

Figure 6. RMS spot radius v.s. perturbation for the on-axis (solid red) and off-axis (dashed blue) with respect to the as-built performance criterion (dotted black). The top two rows show the sensitivity to perturbation in 6DOF for the secondary mirror, whereas the bottom two rows report the tertiary mirror's sensitivity. The intersection of the red or blue line with the dotted black line indicates the perturbation required to increase the spot radius to 0.225 arcseconds.

While the off-axis system's nominal performance is superior, it is clearly more sensitive to misalignment across most degrees of freedom. This can add risk and cost to the mission but can enable higher nominal resolution. To better understand the nominal performance, the point-spread function of each system must be analyzed.

3. POINT-SPREAD FUNCTION ANALYSIS

To account for the minimal phase aberrations present in the original and off-axis freeform CETUS designs a `ZMXOpticalElement` subclass was written for POPPY that loads the exit pupil of a Zemax optical system into a POPPY `OpticalSystem`. This class assumes that all diffraction effects occur in planes conjugate to the exit pupil and image plane, and computes the field at the image plane with the Fraunhofer diffraction integral.

$$U_{img}(x,y) \propto \int\int_{-\infty}^{\infty} U_o(x',y')P(x',y')e^{i(k_x x' + k_y y')}dx'dy' \tag{3}$$

Where U is a complex scalar field, P is the complex transmission of the exit pupil, and $k_{x/y}$ is the spatial frequency coordinate $= \frac{x/y}{\lambda z}$. This permits analysis of the influence of the primary mirror surface error on the image field, but *not* the effects of intermediate planes. Using the `ZMXOpticalElement` subclass the point-spread functions of the aperture geometries in figure 2 were computed and are shown in the top row of figure 7. The diffraction flares from the spider structure spread the energy from an object point around the corresponding image point, which can inhibit the detection of very faint sources. However, this model of the PSF assumes perfect optical surfaces. To bring the physical optics model of the CETUS telescope closer to reality a surface error is assigned to the primary mirror of each optical system. The surface error data used in this comparison comes from a 4.23m primary polished at the University of Arizona - the Daniel K. Inoyue Solar Telescope (DKIST). The surface data was obtained by SCOTS (Software Configurable Optical Test System), a deflectometry measurement machine for large mirrors.[7] A circular section of the DKIST primary was taken corresponding to the $1.5m$ CETUS primary diameter and converted into a fits object via the `astropy` python package. The surface error is shown in figure 8. This allows for the surface data to be included in the physical optics model as a `FITSOpticalElement` in Poppy. The PSFs for the optical system that considers nominal aberration, secondary obscuration, and primary surface roughness are shown in bottom row of figure 7. The PSF analysis thus far qualitatively reveals what a geometrical treatment cannot: that the presence of structure (spiders, surface error) in the pupil plane will corrupt the ability of the observatory to be sensitive to faint sources. An integrated azimuthal average of each PSF gives a more quantitative perspective of how the energy spreads with structure in the pupil. The 50% encircled energy radius was computed for each PSF in figure 7 and is given in table 1.

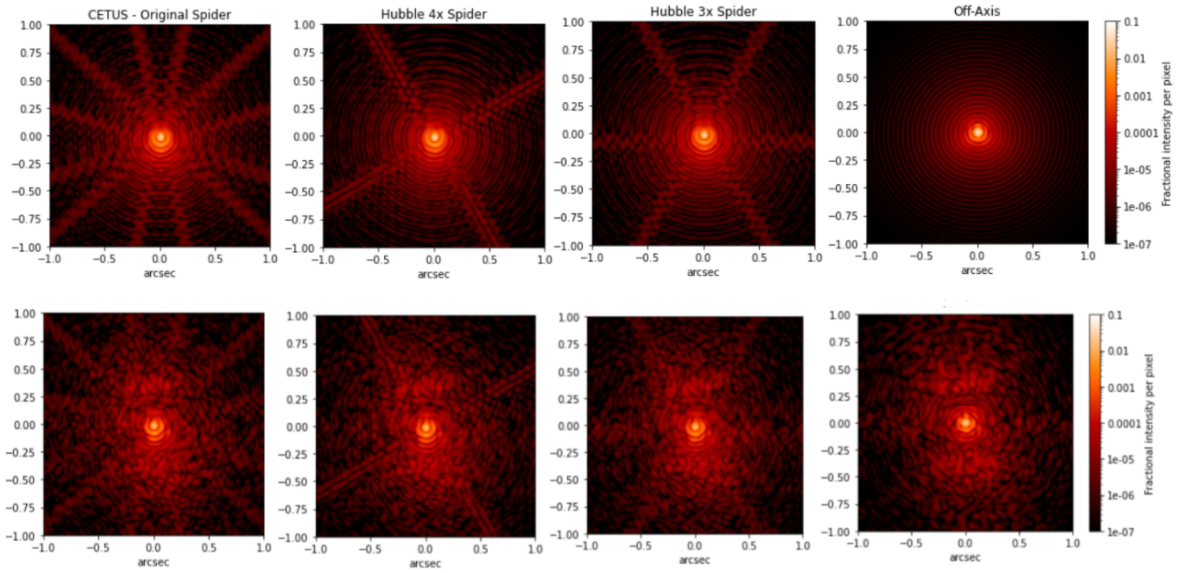

Figure 7. The point-spread functions of the aperture geometries in figure 2 computed at $\lambda = 300nm$. From left to right: The Original CETUS aperture, a Hubble-like aperture with 4 spokes, a Hubble-like aperture with 3 spokes, an unobscured aperture. The PSFs on the top row correspond to a model assuming perfect mirrors, whereas the bottom row includes the surface error of a 1.5m section of the DKIST primary mirror.

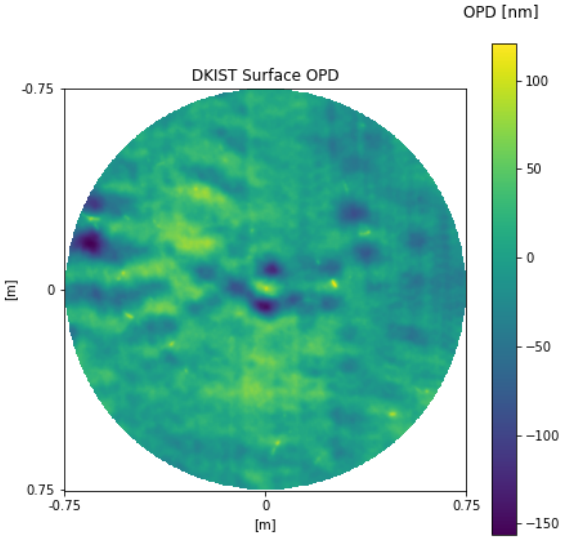

Figure 8. The 1.5m diameter section of the 4.23m DKIST primary used in the computation of the PSFs in figure7.

	Original	Hubble 4x	Hubble 3x	LAF-TMA
50% EE radius w/ ideal mirror	0.061”	0.053”	0.053”	0.025”
50% EE radius w/ DKIST primary	0.206”	0.149”	0.143”	0.069”

Table 1. 50% encircled energy radius of each PSF shown in figure 7. An unaberrated airy disk from a circular pupil has a 50% encircled energy radius of 0.021”. Looking along the rows of the table illustrates the ramifications of the pupil on the image quality, whereas the columns show the degradation due to a rough primary mirror.

This PSF analysis is a very useful step toward understanding the performance of a diffraction-limited system, but this only captures the instrument's response to an unresolved source on-axis. CETUS's wide field of view is capable of capturing extended scenes, and to model how these scenes are captured a source field must be simulated. The instrument's response to a source field is derived convolution theorem of Fourier transforms. A linear and shift-invariant instrument will produce an image plane composed of the PSF convolved with the object, which is a product of the spatial frequency content of the scene with the pupil function in the fourier domain.

$$U_{img}(r,\theta) = U_{obj}(r,\theta) * PSF(r,\theta) = FT^{-1}(FT[U_{obj}(r,\theta)]\dot{F}T[PSF(r,\theta)]) \tag{4}$$

For a preliminary analysis the source field U_{obj} will be a simple field of unresolved stars, modeled as delta functions ($\delta_i(r_i,\theta_i)$) of uniformly random distribution and brightness (A_i).

$$U_{obj}(r,\theta) = \sum_{i}^{N} A_i \delta_i(r_i,\theta_i) \tag{5}$$

Three starfield cases were explored in this study: A starfield with no primary mirror surface error, the DKIST surface error from figure 8, and the DKIST surface error with the first 36 Fringe-indexed Zernike polynomials subtracted from the surface. The latter case gives insight into how the performance may improve if these low-frequency terms are effectively polished out of the mirror.

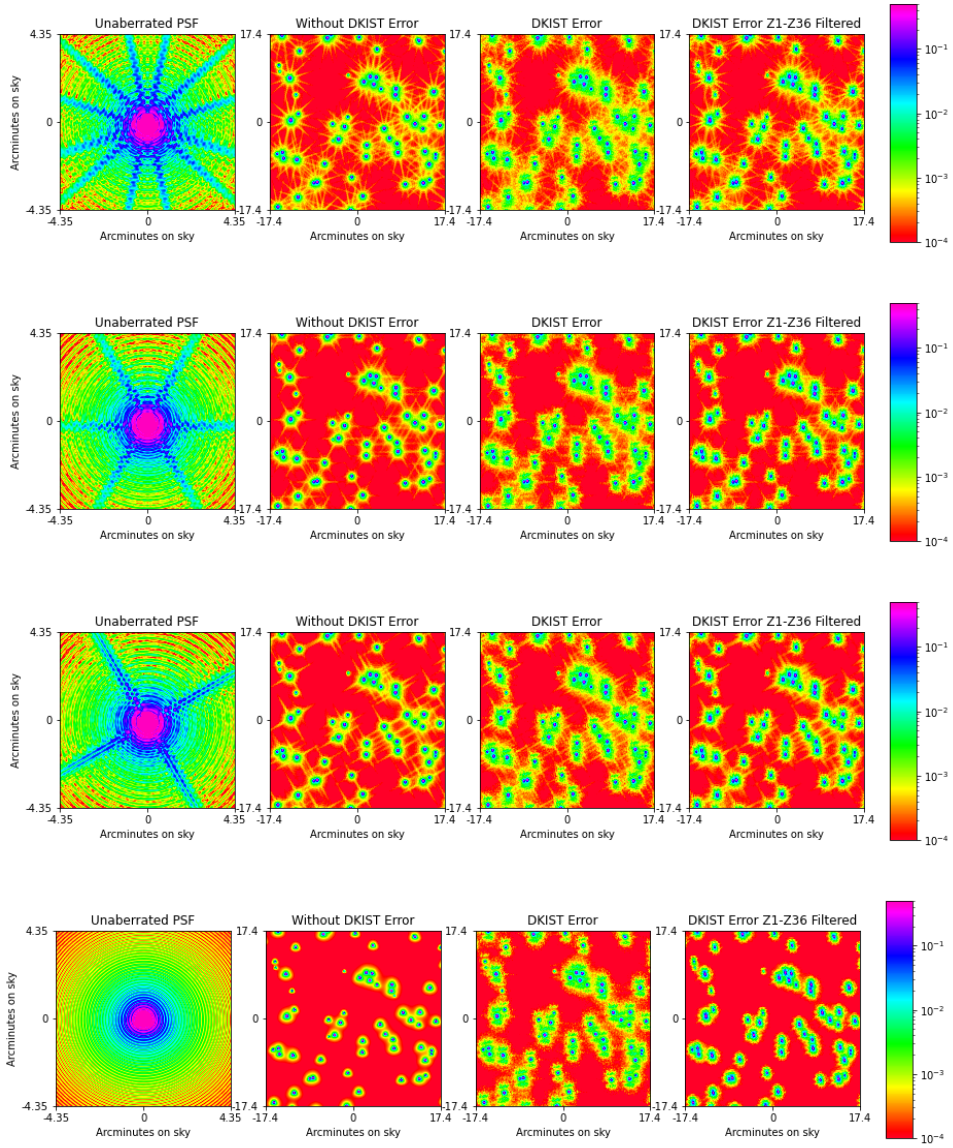

Figure 9. Convolutions of the instrument PSF (Left) of a starfield with a perfect primary mirror (Center Left), the DKIST mirror error (Center Right), and the high-pass filtered DKIST mirror error (Left). This demonstrates the influence of mirror error on the image field with a more realistic instrument model.

The results in figure 9 qualitatively illustrate the considerable influence of the DKIST surface error on the imaging of clustered point sources. Faint objects in the image plane become obscured by more luminous objects nearby. This effect is mitigated in the high-pass filtered case where the halos produced by the rough primary diminish. This study demonstrates that physical optics modeling of diffraction-limited spaceborne optical systems can provide greater insight into the anticipated performance of the optical system.

4. CONCLUSION

The original CETUS fore-optics are evaluated against an alternative system designed with insights from linear-astigmatism free optical systems. The alignment sensitivity of each design is compared for insights into the necessary optomechanical tolerances upon assembly of the optical system. Various pupil geometries are explored and their diffraction performance is analyzed with both perfect mirrors and an imperfect primary mirror. This study shows that new geometrical optical solutions can enable more diffraction-optimized optical systems, at the cost of greater sensitivity to misalignment. The optical modeling effort of CETUS will continue in order to further understand the optical trade spaces with consideration for diffraction to further refine the observatory's optical systems.

5. FUTURE WORK

5.1 Field-dependent convolution

The scene convolution done in this study was conducted assuming that CETUS was linear and shift-invariant, but a glance at figure 4 would reveal that this is not necessarily the case. The small wavefront error is a function of the field of view, which will shape the PSF differently across the FoV. The high nominal performance of the system means that the difference is small (as shown in figure 10).

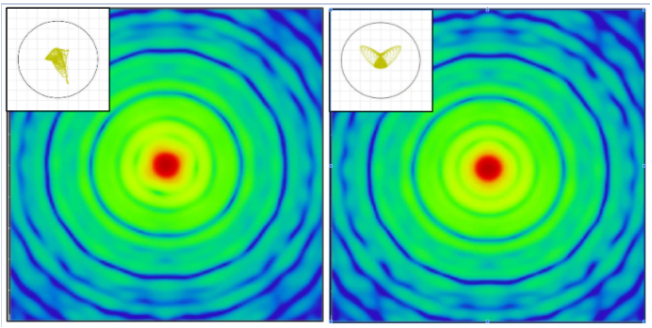

Figure 10. PSF computed at the edge (left) an center (right) of the CETUS FoV. The geometrical spots are shown in the top left of each PSF. The slight differences manifest most noticeably in the core of the PSF, indicating that the PSF will change slightly over the FoV.

To accommodate for this shift a separate convolution can be done for each point in the field of view. While computationally intensive, such a simulation permits a greater understanding of how different points in the image plane evolve across the field of view. Such a simulation has been accelerated by using linear interpolations of the PSFs across the field of view for the Roman-CGI Hybrid Lyot Coronagraph.[8]

5.2 Speckle Propagation w/ `FresnelOpticalSystem`

The PSF analysis only captured diffraction effects from structure in pupil planes. While significant, modeling imperfections from all optical elements in the system would produce a more realistic simulation of the anticipated field at the image plane. Poppy has support for plane-to-plane diffraction using Fresnel Diffraction[9] that permit the propagation of speckle from mirror to mirror. A rough optical surface can be assigned to the secondary and tertiary mirrors to evaluate their influence on the image plane and tolerance the manufacturing error to achieve the desired resolution.

5.3 Real-Scene Simulations of Diffuse Sources

The method outlined in section 3 and 5.1 can be applied to any scene of interest. Given a model of the spatial distribution and surface brightness of a CGM-like object, the field incident on the detector can be modeled for a full analysis of the detectability of diffuse extended sources. Tracing the power through the optical model would allow analysis of the actual power expected to be incident on the detector.

ACKNOWLEDGMENTS

This research made use of community-developed core Python packages, including: Numpy,[10] Matplotlib,[11] SciPy,[12] Jupyter, IPython Interactive Computing architecture.[13,14] This research also used POPPY, an open-source optical propagation Python package originally developed for the James Webb Space Telescope project (Perrin, 2012).[4]

REFERENCES

[1] Heap, S., Arenberg, J., Hull, T., Kendrick, S., and Woodruff, R., "The nasa probe space mission concept, cosmic evolution through uv surveys (cetus)," (2019).

[2] Abraham, R., van Dokkum, P., Conroy, C., Merritt, A., Zhang, J., Lokhorst, D., Danieli, S., and Mowla, L., "Future prospects: Deep imaging of galaxy outskirts using telescopes large and small," *Outskirts of Galaxies* , 333–358 (2017).

[3] Krist, J., "Simulation of HST PSFs using Tiny Tim," in [*Astronomical Data Analysis Software and Systems IV*], Shaw, R. A., Payne, H. E., and Hayes, J. J. E., eds., *Astronomical Society of the Pacific Conference Series* **77**, 349 (Jan. 1995).

[4] Perrin, M. D., Soummer, R., Elliott, E. M., Lallo, M. D., and Sivaramakrishnan, A., "Simulating point spread functions for the James Webb Space Telescope with WebbPSF," in [*Space Telescopes and Instrumentation 2012: Optical, Infrared, and Millimeter Wave*], Clampin, M. C., Fazio, G. G., MacEwen, H. A., and Jr., J. M. O., eds., **8442**, 1193 – 1203, International Society for Optics and Photonics, SPIE (2012).

[5] Feng, Y.-T., Ashcraft, J. N., Breckinridge, J. B., Harvey, J. E., Douglas, E. S., Choi, H., Lillie, C., Hull, T., and Kim, D. W., "Topological pupil segmentation and point spread function analysis for large aperture imaging systems," in [*AOPC 2020: Optics Ultra Precision Manufacturing and Testing*], Kong, L., Zhang, D., and Luo, X., eds., **11568**, 105 – 117, International Society for Optics and Photonics, SPIE (2020).

[6] Sasián, J., "Method of confocal mirror design," *Optical Engineering* **58**(1), 1 – 12 (2019).

[7] Huang, R., Su, P., and Burge, J. H., "Deflectometry measurement of Daniel K. Inouye Solar Telescope primary mirror," in [*Optical Manufacturing and Testing XI*], Fähnle, O. W., Williamson, R., and Kim, D. W., eds., **9575**, 195 – 209, International Society for Optics and Photonics, SPIE (2015).

[8] Milani, K. and Douglas, E. S., "Faster imaging simulation through complex systems: a coronagraphic example," in [*Optical Modeling and Performance Predictions XI*], Kahan, M. A., ed., **11484**, 15 – 28, International Society for Optics and Photonics, SPIE (2020).

[9] Douglas, E. S. and Perrin, M. D., "Accelerated modeling of near and far-field diffraction for coronagraphic optical systems," *Space Telescopes and Instrumentation 2018: Optical, Infrared, and Millimeter Wave* (Jul 2018).

[10] Harris, C. R., Millman, K. J., van der Walt, S. J., Gommers, R., Virtanen, P., Cournapeau, D., Wieser, E., Taylor, J., Berg, S., Smith, N. J., Kern, R., Picus, M., Hoyer, S., van Kerkwijk, M. H., Brett, M., Haldane, A., del Río, J. F., Wiebe, M., Peterson, P., Gérard-Marchant, P., Sheppard, K., Reddy, T., Weckesser, W., Abbasi, H., Gohlke, C., and Oliphant, T. E., "Array programming with NumPy," *Nature* **585**, 357–362 (Sept. 2020).

[11] Hunter, J. D., "Matplotlib: A 2d graphics environment," *Computing in Science & Engineering* **9**(3), 90–95 (2007).

[12] Jones, E., Oliphant, T., and Peterson, P., "SciPy: Open source scientific tools for Python," *http://www.scipy. org/* (2001).

[13] Pérez, F. and Granger, B., "IPython: A System for Interactive Scientific Computing," *Computing in Science Engineering* **9**, 21–29 (May 2007).

[14] Kluyver, T., Ragan-Kelley, B., Pérez, F., Granger, B. E., Bussonnier, M., Frederic, J., Kelley, K., Hamrick, J. B., Grout, J., and Corlay, S., "Jupyter Notebooks-a publishing format for reproducible computational workflows.," in [*Positioning and Power in Academic Publishing: Players, Agents and Agendas*], 87–90 (2016).